ADVANCED ENERGY MATERIALS
www.advenergymat.de

Multi-Mode Vibrational Triboelectric Nanogenerator for Broadband Energy Harvesting and Utilization in Smart Transmission Lines

Xiaosong Zhang, Yang Yu, Xiao Xia, Weiqi Zhang, Xiaojun Cheng, Hengyu Li, Zhong Lin Wang,* and Tinghai Cheng**

The advantages of the triboelectric nanogenerator (TENG) in environmental energy harvesting and utilization determine that they have great development potential in the digital application of power grids. This work focuses on the harvesting and utilization of vibration energy from transmission lines, specifically in the context of breeze vibrations and sub-span oscillations. To this end, this work proposes a novel multi-mode vibrational triboelectric nanogenerator (MV-TENG) and three smart transmission line application strategies based on the MV-TENG. The MV-TENG design consists of an S-beam to broaden the frequency response range by reducing high-order modal frequencies, and a pair of allegro electrodes to efficiently harvest horizontal and vertical vibration energy. The MV-TENG demonstrates the capability to harvest vibration energy within a range of 1–3.5 Hz horizontally and 4 Hz, 9–60 Hz vertically, covering the occurrence range of breeze vibrations and sub-span oscillations of transmission line effectively. Three application strategies include self-powered tower obstacle alerting, temperature and humidity online monitoring, and high-temperature wireless warning of transmission lines based on MV-TENG. In summary, this work presents a comprehensive implementation scheme for digitally integrating TENGs into smart transmission lines, thereby facilitating the engineering development of TENG technology in grid systems.

1. Introduction

The increasing intelligence of grid systems has created a growing demand for digital monitoring devices.[1,2] As pivotal components in smart grid systems, the transmission lines play a crucial role in long-distance energy delivery.[3] The traditional digital monitoring devices of the transmission lines mostly rely on chemical batteries for power supply. However, the drawbacks of frequent replacements, high operational costs, and environmental pollution associated with chemical batteries have become increasingly apparent.[4–6] The surging demand for digital monitoring in power transmission has rendered chemical batteries inadequate to meet current technical requirements. Given this, the adoption of small generators to collect energy from the working environment of the transmission lines and then power the digital monitoring devices emerges as a viable solution.[7–9] Currently, most sensing and warning devices in the transmission lines are powered by solar power. Years of practical applications have found that the efficiency of solar energy harvesting is easily affected by rainy weather and contaminants on the surface of solar panels. It easily leads to insufficient power supply during a long-term run, resulting in the equipment being unable to work stably, which affects the reliability of the sensing systems.[10,11] In addition, the wind generator and current transformer (CT) have also been demonstrated to obtain abundant environmental energy in the working environment of the transmission lines, but also have significant disadvantages. The wind generator can not efficiently generate electricity under a low wind speed range. The CT has the problems of power supply dead band and core saturation, and the application scenarios are limited. Thus, the development of a novel and sustainable method for environmental energy harvesting in smart transmission lines becomes an urgent priority.

The emergence of triboelectric nanogenerator (TENG) based on triboelectric and electrostatic induction effects has revolutionized the way of environmental energy harvesting and

X. Zhang, Y. Yu, X. Xia, W. Zhang, X. Cheng, H. Li, Z. L. Wang, T. Cheng
Beijing Institute of Nanoenergy and Nanosystems
Chinese Academy of Sciences
Beijing 101400, P. R. China
E-mail: lihengyu@binn.cas.cn; zhong.wang@mse.gatech.edu; chengtinghai@binn.cas.cn
X. Zhang, Y. Yu, X. Cheng, H. Li, T. Cheng
Scchool of Nanoscience and Engineering
University of Chinese Academy of Sciences
Beijing 100049, P. R. China
Z. L. Wang
Georgia Institute of Technology
Atlanta, GA 30332, USA
Z. L. Wang
Yonsei Frontier Lab
Yonsei University
Seoul 03722, Republic of Korea

The ORCID identification number(s) for the author(s) of this article can be found under https://doi.org/10.1002/aenm.202302353

DOI: 10.1002/aenm.202302353

utilization. Since the invention by Wang's group in 2012,[12] TENG technology has been widely used in micro-nano energy harvesting,[13–15] self-powered sensing[16–18] and other fields. Capitalizing on Maxwell's displacement current, the TENG can convert various forms of mechanical energy in the surrounding environment into electrical energy, including wind energy,[19–21] water energy,[22,23] and vibration energy.[24–26] Researchers have successfully employed TENGs to power various small electronic devices, such as temperature and humidity sensors,[27] anemometers,[28] and light sensors.[29] On the other hand, the transmission lines are usually designed with large spans and elevated structures, and so that the wires are prone to the periodic vibrations induced by wind action.[30,31] These periodic vibrations mainly manifest as the vertical breeze vibration and the horizontal sub-span oscillation and gallop. In response, some researchers have explored the application of TENGs for harvesting vibration energy in transmission lines.[32–34] Wu et al. presented a vibration-driven triboelectric nanogenerator for harvesting breeze vibration energy of transmission lines, enabling the powering of low-power sensors while dampening the transmission line vibrations.[35] Additionally, Gao et al. proposed a triboelectric–electromagnetic hybridized generator for harvesting the galloping energy from transmission lines and monitoring their galloping state.[36] Notably, the vibration frequency and amplitude range of transmission lines are different in vertical and horizontal directions. However, it is difficult for the current research to achieve a broadband response for vibration energy harvesting in both directions simultaneously.

Herein, a S-shaped multi-mode vibrational triboelectric nanogenerator (MV-TENG) is designed. Among them, the S-beam adopts the arc cantilever beam series connection method to obtain broadband vibration characteristics for the MV-TENG. In addition, an allegro electrode structure is designed according to the angular arc swing characteristics of the s-beam end, and a vertical contact-separation mode TENG is integrated into the allegro electrode. This innovation enables MV-TENG to quickly respond to horizontal and vertical vibrations and efficiently harvest their energy. This one-piece structure design has the characteristics of a simple structure and is lightweight, which reduces the installation complexity of MV-TENG. The research commences with a modal analysis of the MV-TENG characteristics, coupled with a detailed explanation of the working mechanism of allegro electrodes and an optimized process of the S-beam structure. A non-parallel vertical contact-separation mode theory model is proposed to provide a comprehensive understanding of the MV-TENG. The horizontal and vertical vibration experimental systems are built. The prototypes of arc TENG and MV-TENG are developed and their basic output performances are measured. The MV-TENG demonstrates the capability to harvest vibration energy within a range of 1–3.5 Hz horizontally and 4 Hz, 9–60 Hz vertically. Furthermore, the coupling output performance and mean power of the MV-TENG are studied, which can reach 435.093 and 459.734 μW in the horizontal and vertical directions, respectively. Finally, three application strategies in transmission lines are proposed, and the technical feasibility of the MV-TENG in digitalization applications of the smart grid is verified through a series of demonstrations.

2. Results and Discussion

2.1. Structural Design and Working Mechanism of the MV-TENG

To realize vibration energy harvesting of both horizontal and vertical directions caused by breeze vibration and sub-span oscillation of transmission lines, a simple multi-mode vibrational triboelectric nanogenerator (MV-TENG) is designed. The layout and detailed structure of the MV-TENG on the transmission line are shown in **Figure 1**a. The MV-TENG can collect vibration energy in two orthogonal directions just by utilizing an S-shaped beam (S-beam) and allegro electrodes. Among them, the S-beam adopts the arc cantilever beam series connection method to realize the broadband vibration of the MV-TENG. Considering that the end corner of the S-beam is an arc-shaped swing, the allegro electrodes are designed. The design of the electrodes is inspired by the traditional Chinese art instrument "Allegro" and incorporates a vertical contact-separation mode TENG within the allegro structure. This innovation allows the MV-TENG to respond to both horizontal and vertical vibrations efficiently. Among them, the allegro electrodes consist of a bottom plate electrode and an upper plate electrode. The bottom plate electrode is located on the corner side plates of the S-beam and motion with the vibration deformation of the S-beam. The bottom plate electrode is successively covered with sponge, copper foil and fluorinated ethylene propylene (FEP) film. A polylactic acid (PLA) plate of the upper plate electrode is mounted on the corner side of the S-beam through a hinge structure. The sponge, copper foil, and nylon film are successively attached to the PLA plate of the upper electrode. Here, the copper foil serves as electrodes and the FEP and nylon act as two triboelectric layers with opposite triboelectric polarity. The sponge acts as a cushioning material to enhance the planar contact effect of the allegro electrodes and reduce the impact of the collision on the MV-TENG. The MV-TENG features a pair of allegro electrodes at each of the three corners. The MV-TENG can be arbitrarily distributed on transmission lines to collect the vibration energy of transmission lines and power low-power sensing and warning devices in the grid, enabling self-powered status monitoring of transmission lines.

Figure 1b shows a schematic diagram of the energy conversion and corresponding motion mechanism of the MV-TENG. The frequency range of breeze vibration of transmission lines is mainly 3–50 Hz, and the amplitude is not more than 2 times the diameter of the transmission line (≈50 mm).[37] Excited by the breeze vibration, the MV-TENG is subjected to vertical vibrations that bend the S-beam, causing the three allegro electrodes to open and close (Figure 1b(i)). Conversely, the frequency range of sub-span oscillation of transmission lines is generally 1–3 Hz, and the amplitude is generally 0.1–0.5 m.[38] Under the excitation of the sub-span oscillation, the MV-TENG is subjected to horizontal vibration to cause the upper plate electrode of allegro electrodes to move due to inertia, so that the three allegro electrodes are opened and closed (Figure 1b(ii)). Based on triboelectric and electrostatic induction effects, the MV-TENG converts external mechanical energy generated by the breezy vibration and sub-span oscillation into electrical energy during the opening and closing motion of the allegro electrodes.

To verify the motion mechanism of the MV-TENG and illustrate the broadband response characteristics of the MV-TENG, a

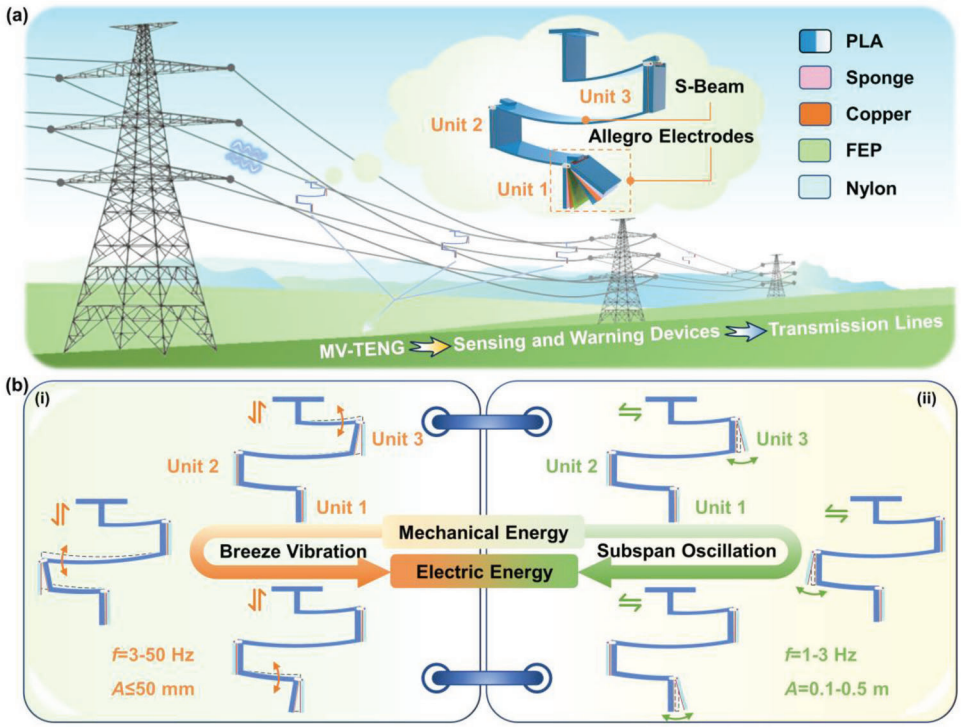

Figure 1. Structural design of the MV-TENG. a) Layout of transmission lines and detailed structure of the MV-TENG. b) Schematic diagrams of the energy conversion and corresponding motion mechanism of the MV-TENG.

series of modal simulations about beams with different layers are carried out. The modal contours are shown in **Figure 2**a. The end corners of the one-layer beam, two-layer beam, and three-layer beam produce arc-shaped swings under the vertical vibration. Video S1 (Supporting Information) records the simulated motion process. In addition, the first 20 modes under the three structures are simulated and the results are shown in Figure 2b. It is clear that the number of modes in the low-frequency range also increases when the number of beam layers increases. The specific modal frequencies in the range of 0–60 Hz are shown in **Table 1**. To enhance the frequency response range of the MV-TENG under the breeze vibrations of transmission lines (3–50 Hz), the three-layer beam is selected as the S-beam structure of the MV-TENG. In addition, the modal of S-beams with different widths are analyzed. As shown in Figure S1 (Supporting Information), as the beam width increases, the modal frequency shows an upward trend, but the changed values are very small. The width of the beam determines the size of the TENG. The larger the size of the TENG, the better the output performance. However, if the length-to-width ratio of the beam is too small, it does not meet the theoretical calculation conditions of the beam, thereby a large error may be introduced. Therefore, the width of the S-beam is chosen to be 60 mm.

The MV-TENG adopts the vertical contact-separation mode and the working mechanism is shown in Figure 2c. The bottom and upper plate electrodes of allegro electrodes are constantly opened and closed under the vibration excitation. There are three typical locations in the entire power harvesting process. In the initial stage, the allegro electrodes are in full contact. Based on the principle of contact electrification and electrostatic induction effects, the FEP and nylon film surfaces produce equal amounts of opposite charge. During the opening stage, the allegro electrodes begin to separate. The original electrostatic equilibrium is broken, and a potential difference occurs between copper electrodes due to electrostatic induction. The potential difference causes electrons to move directionally between the two copper electrodes, creating a new electrostatic equilibrium. During this process, a current with the opposite direction of electron movement is formed in the external load (Figure 2c(i)). In the maximum opening position stage, the distance between the two electrodes is maximized. At this point, the amount of transferred charge and the value of the voltage reach a maximum value at the same time. And the current is zero as there is no longer any transfer of electrons. When the allegro electrodes are closed, the external load creates a current opposite to the opening process of the allegro electrodes (Figure 2c(ii)). When the allegro electrodes return to the original position, the initial electrostatic equilibrium is re-established. This is a complete process of the MV-TENG generating a periodic electrical signal. When the external vibrations are continuously excited, the MV-TENG generates a continuous cycle of power generation that enables continuous vibration energy harvesting. To better illustrate the working mechanism of the MV-TENG in continuous vibration, the potential distribution of allegro electrodes at three typical angles is simulated using COMSOL software (Figure S2a, Supporting Information), and probes are used for fixed-point potential monitoring (Figure S2b, Supporting Information). The simulated power generation process is consistent with the working mechanism shown in Figure 2c. In addition, the real output curves of the allegro electrodes shown in Figure 2d further verify the above working mechanism.

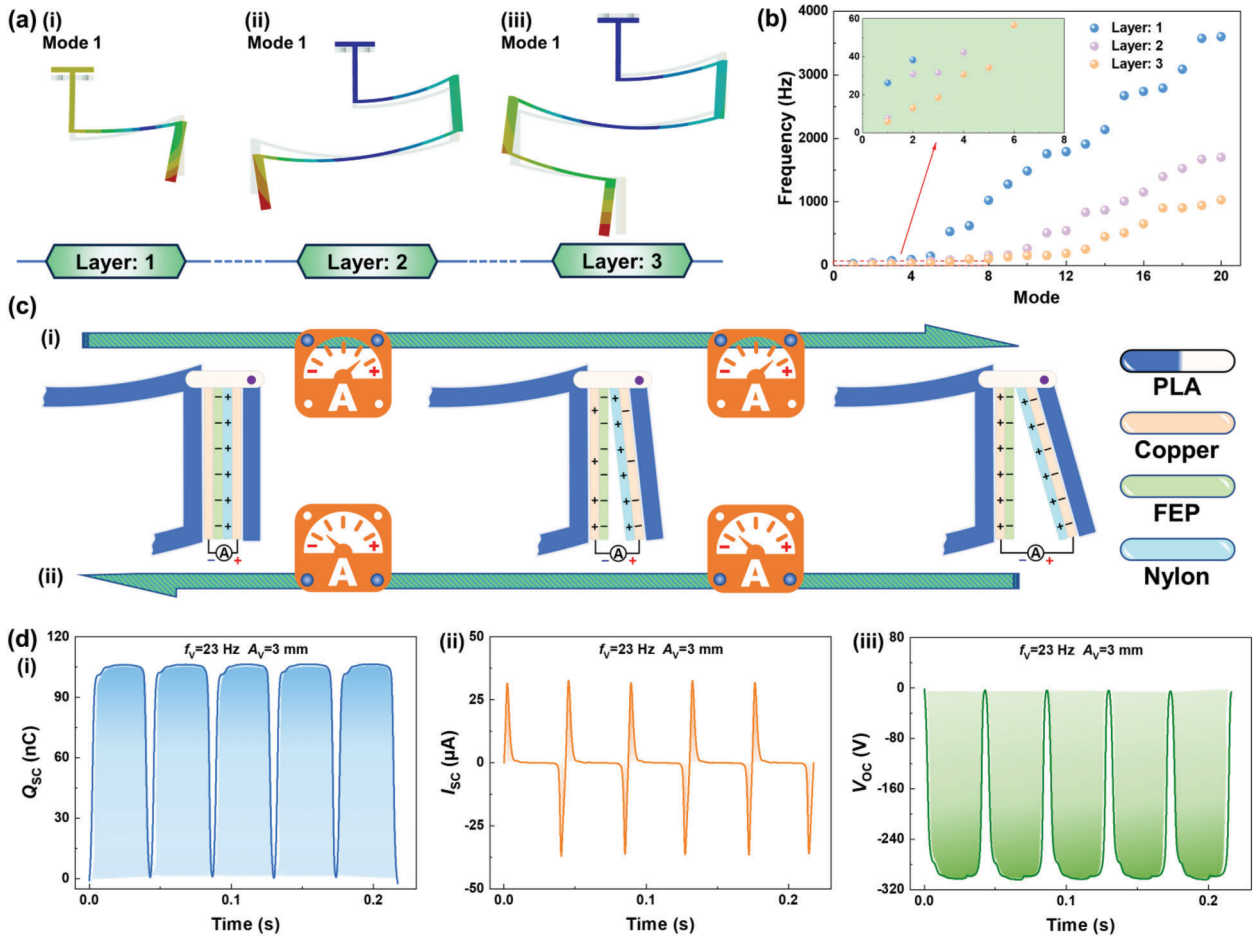

Figure 2. Working mechanism analysis of the MV-TENG. a) Contours of first-order modal and b) modal simulation frequency results of beams with different layers. c) Charge transfer process of allegro electrodes under i) opening and ii) closing stages. d) Output curves of the prototype.

2.2. Model Analysis of the MV-TENG

A non-parallel vertical contact-separation mode theory model is developed to explain the working mechanism of allegro electrodes with deflection motion. Since the allegro electrodes are non-parallel motion, the inside electric field of electrodes is non-uniform. From the electrostatic field loop theorem, the electric field lines at the proximal end of the two electrodes are denser than those at the far end (Figure S3, Supporting Information). The extension wires of the electrodes A and B intersect at point O with an angle of θ ($\theta \leq 180°$). The electric potential between two electrodes at the deflection center axis O distance r is:

$$U_r = E(r)\, r\theta \tag{1}$$

where $E(r)$ is the electric field strength and $r\theta$ is the arc electric field line length.

The area between the two electrodes A and B is considered to be a large number of arc-shaped units connected in parallel. The electric field energy of any arc-shaped unit can be expressed as:

$$\mathrm{d}W = \frac{1}{2}\varepsilon_0 E^2(r)\,\mathrm{d}V = \frac{1}{2}\varepsilon_0 l \frac{U_r^2}{r\theta}\mathrm{d}r \tag{2}$$

where ϵ_0 is the vacuum permittivity, and l is the length of the electrode. Therefore, the energy of the electric field inside the entire allegro electrodes is:

$$W = \int_V \mathrm{d}W = \frac{1}{2}\varepsilon_0 l \frac{U_r^2}{\theta} \ln\frac{R_2}{R_1} \tag{3}$$

where R_1 and R_2 are the closest and farthest distances from the electrode to point O, respectively. The capacitance of the allegro electrodes solved is:

$$C = \frac{2W}{U^2} = \frac{\varepsilon_0 l}{\theta}\ln\frac{R_2}{R_1} \tag{4}$$

The angle θ is a function of time t during the movement of the allegro electrodes. Suppose the amount of charge carried by the two electrodes is Q. Then the potential difference U of the two electrodes during motion can be expressed as:

$$U = \frac{Q}{C} = \frac{Q}{\varepsilon_0 l\left(\ln R_2 - \ln R_1\right)}\theta(t) \tag{5}$$

Table 1. Modal frequencies in the range of 0–60 Hz (Unit: Hz).

Mode	1	2	3	4	5	6
Layer-1	26.264	38.219	N/A	N/A	N/A	N/A
Layer-2	7.757	30.79	31.599	42.353	N/A	N/A
Layer-3	5.881	13.012	18.511	30.639	34.249	56.556

From the above equations, the value of the potential difference of the allegro electrodes increases with the increase of the opening angle, which verifies the previous analysis. More specific processes can be found in Equations S1–S9 (Supporting Information).

2.3. Basic Output Performances of the MV-TENG

To verify the feasibility of combining the arc cantilever beam with the allegro electrodes to achieve vibration energy harvesting in two directions, an arc TENG with a one-layer beam is developed. The prototype photographs and the excitation systems in two vibration directions are shown in **Figure 3**a. The linear motor is used to simulate horizontal vibration excitation and the electrodynamic shaker is used to simulate vertical vibration excitation. The output performances of arc TENG under different amplitudes are studied, and the results are shown in Figure 3b and Figure S3 (Supporting Information). The output performances in horizontal and vertical vibration directions increase with the increase of amplitude, and the performance changing trend in vertical vibration is more obvious. Therefore, it is preliminarily proved that the design method can achieve energy harvesting under horizontal and vertical vibration directions. The 100 mm horizontal vibration amplitude and 3 mm vertical vibration amplitude meet the vibration conditions of the transmission line. Therefore, the subsequent experiments are carried out with a horizontal vibration amplitude of 100 mm and a vertical vibration amplitude of 3 mm. Subsequently, the vibration frequency response of the arc TENG is studied. The vibration frequency response of the arc TENG in the horizontal direction is shown in Figure 3c and Figure S4 (Supporting Information). In the 0.5–3.5 Hz vibration range, the output performance of the arc TENG increases with increasing frequency. It shows that the arc TENG can realize energy harvesting

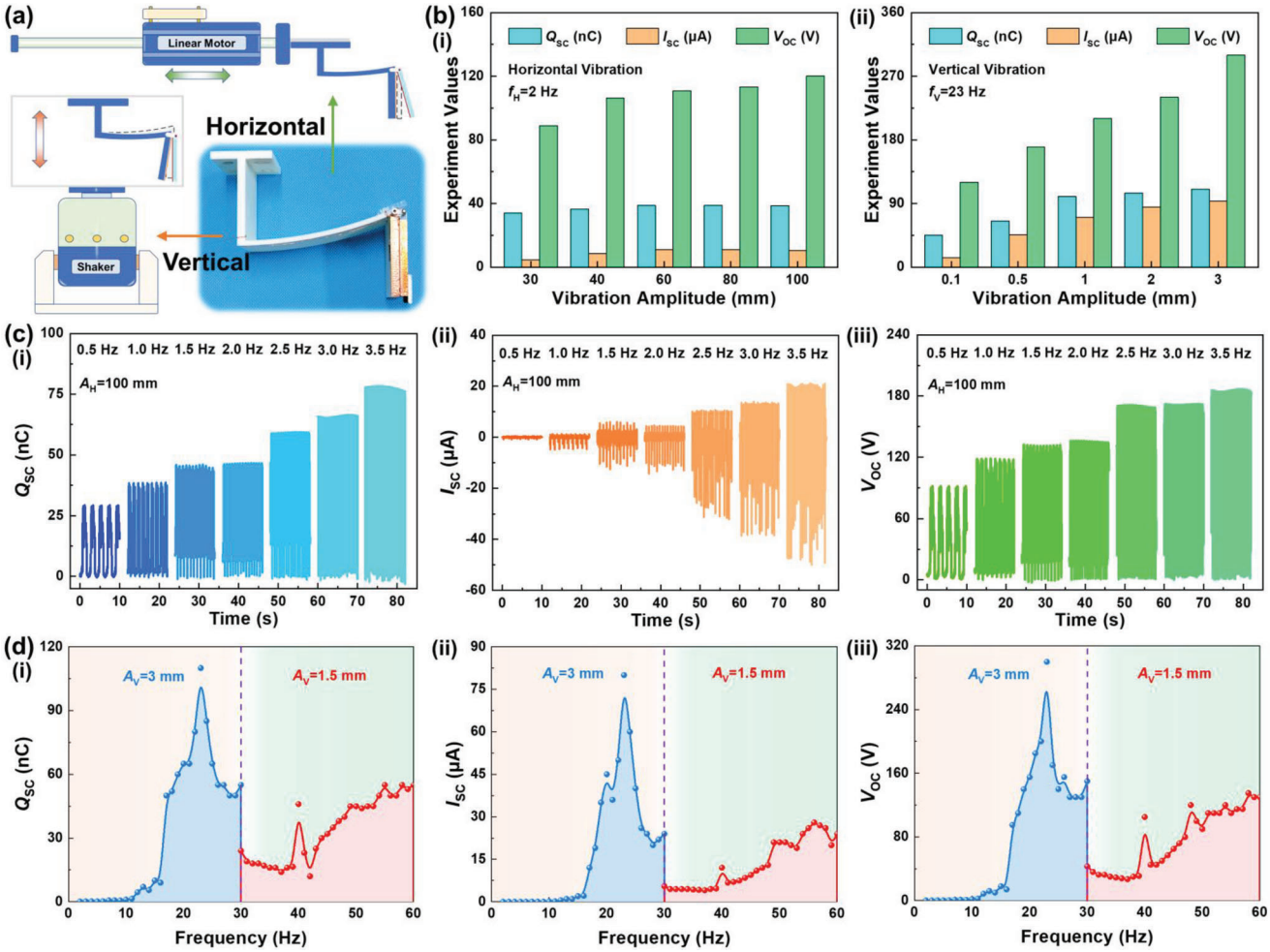

Figure 3. Output performance of arc TENG. a) Schematic diagrams of horizontal and vertical vibration excitation systems. b) Output performances of arc TENG with different amplitudes under i) horizontal and ii) vertical vibrations. c) Output performances of arc TENG with different vibration frequencies under horizontal and d) vertical.

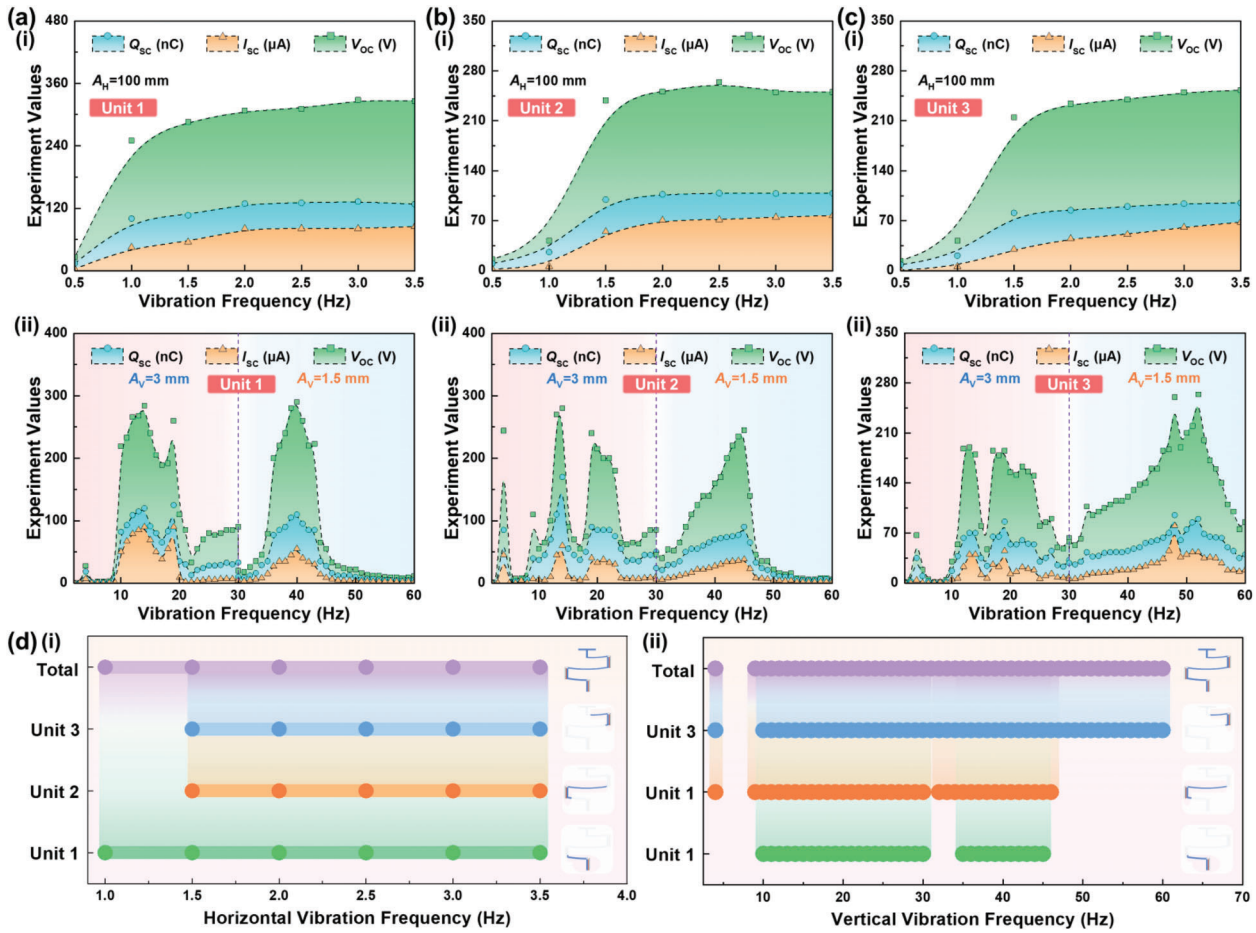

Figure 4. Output performance of the MV-TENG. a) Output performances of unit 1 with different vibration frequencies in i) horizontal and ii) vertical directions. b) Output performances of unit 2 with different vibration frequencies in i) horizontal and ii) vertical directions. c) Output performances of unit 3 with different vibration frequencies in i) horizontal and ii) vertical directions. d) Frequency response range of the MV-TENG under i) horizontal and ii) vertical vibration directions.

within the vibration range of the sub-span oscillation in transmission lines. In addition, the arc TENG can also achieve horizontal vibration energy harvesting in the high-frequency range of 10–50 Hz (Figure S5, Supporting Information). Therefore, this design method can also be applied to high-frequency vibration energy harvesting in other horizontal vibration fields. The vibration frequency response of arc TENG in the vertical direction is shown in Figure 3d and Figure S6 (Supporting Information) The arc TENG has good output performance in the vertical vibration frequency range of 17–60 Hz. This result indicates that the arc TENG can realize energy harvesting within the vibration range of breeze vibration in transmission lines. And the arc TENG has two obvious vibration peak points of 23 and 40 Hz, which are consistent with the simulation results (26.264 and 38.219 Hz) in Table 1. To observe the entire process, the low-speed motion processes of the arc TENG under horizontal and vertical vibration directions are recorded (Video S2, Supporting Information), which clearly shows the feasibility of the design method.

To enhance the frequency response range and further improve the output performance, an MV-TENG with the three-layer beam is developed (Figure S7, Supporting Information). The prototype has the advantages of a simple structure and low weight (255.5 g). In addition, the experimental systems for horizontal and vertical vibration are built as shown in Figure S8 (Supporting Information). Video S2 (Supporting Information) shows the low-speed motion processes of the MV-TENG prototype under horizontal and vertical vibration directions. The three units of the MV-TENG are measured separately, and the results are shown in **Figure 4**a–c. In the horizontal vibration experiment, the output performance of the MV-TENG first increases with the increase of vibration frequency and then tends to stabilize. All units have good output performances in the sub-span oscillating vibration frequency range (1–3 Hz). In the vertical vibration experiment, the three units of the MV-TENG have multiple peak points. Although the peak points of the three units have a slight difference, they are basically concentrated at 4, 14, 19, 30, 40, and 48 Hz. They are basically consistent with the first four-order modal frequencies of the 3-layer beam shown in Table 1 but differ greatly from the modal frequencies of the 5th and 6th orders of that. The main reason for this phenomenon is that higher-order modal analysis is more sensitive to small differences in relevant distribution parameters and local structural details, resulting in the

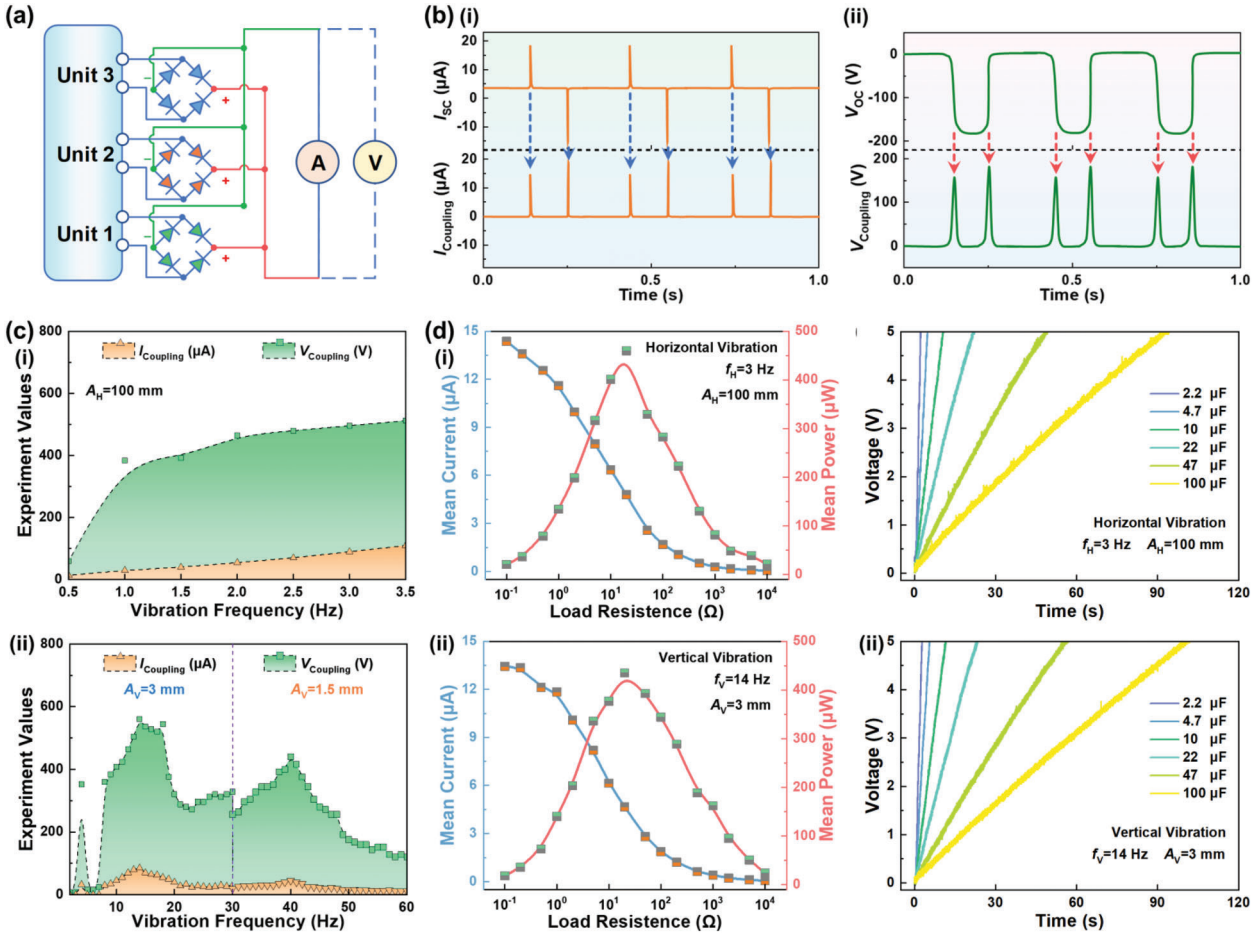

Figure 5. Coupling output performance of the MV-TENG. a) Schematic diagram of the coupling output and measurement circuit. b) Schematic diagrams of the rectification conversion process of voltage and current signals. c) Coupling output performances of the MV-TENG with different frequencies under i) horizontal and ii) vertical vibrations. d) Mean current and power of the MV-TENG on different external loads under i) horizontal and ii) vertical vibrations. e) Charging voltage of the MV-TENG on different capacitors under i) horizontal and ii) vertical vibrations.

experimental results of higher-order modes being far from the simulation results. The actual output curves of the MV-TENG in the horizontal and vertical vibration are shown in Figures S9 and S10 (Supporting Information). According to the experimental results, the vibration frequency response ranges of the MV-TENG in the horizontal and vertical directions are established (Figure 4d). Through the superposition of the frequency response range of the three units, the total frequency response range of the MV-TENG in the horizontal vibration direction is 1–3.5 Hz (Figure 4d(i)), and that in the vertical vibration direction is 4 Hz, 9–60 Hz (Figure 4d(ii)). It is verified that the MV-TENG can realize broadband vibration energy harvesting in both horizontal and vertical directions.

To facilitate the storage and utilization of energy in subsequent applications, a coupling rectifier circuit is designed, and the coupling voltage and current after the MV-TENG rectification are measured. The circuit schematic and signal rectification conversion process are shown in **Figure 5**a,b. The bridge rectifiers are used to convert the AC signals output by the three units into DC signals separately. All waveforms with short-circuit currents I_{SC} less than zero are converted to positive pulse signal waveforms (Figure 5b(i)), while the open-circuit voltage V_{OC} waveforms are converted to positive pulse signal waveforms at the waveform edges (Figure 5b(ii)). Then, all signals are coupled to the output in parallel. The coupling output performances of the MV-TENG under horizontal and vertical vibration directions are shown in Figure 5c and Figure S11 (Supporting Information). The MV-TENG achieves stable and good output in the horizontal vibration frequency range of 1–3.5 Hz (Figure 5c(i)) and the vertical vibration frequency range of 4 Hz and 9–60 Hz (Figure 5c(ii)), which are consistent with the frequency response range of Figure 4d. Subsequently, the average current of the MV-TENG under different external loads is measured and the corresponding average power is calculated. As can be seen from Figure 5d, the mean current gradually decreases as the external load increases. The mean power of the MV-TENG reaches the maximum value when the load resistance is 20 MΩ. Among them, the maximum mean powers corresponding to horizontal and vertical vibration directions are 435.093 and 459.734 μW, respectively. The charging voltage curves of electrolytic capacitors with different capacitances are shown in Figure 5e. When the horizontal vibration frequency is 3 Hz and the amplitude is 100 mm, a 2.2 μF

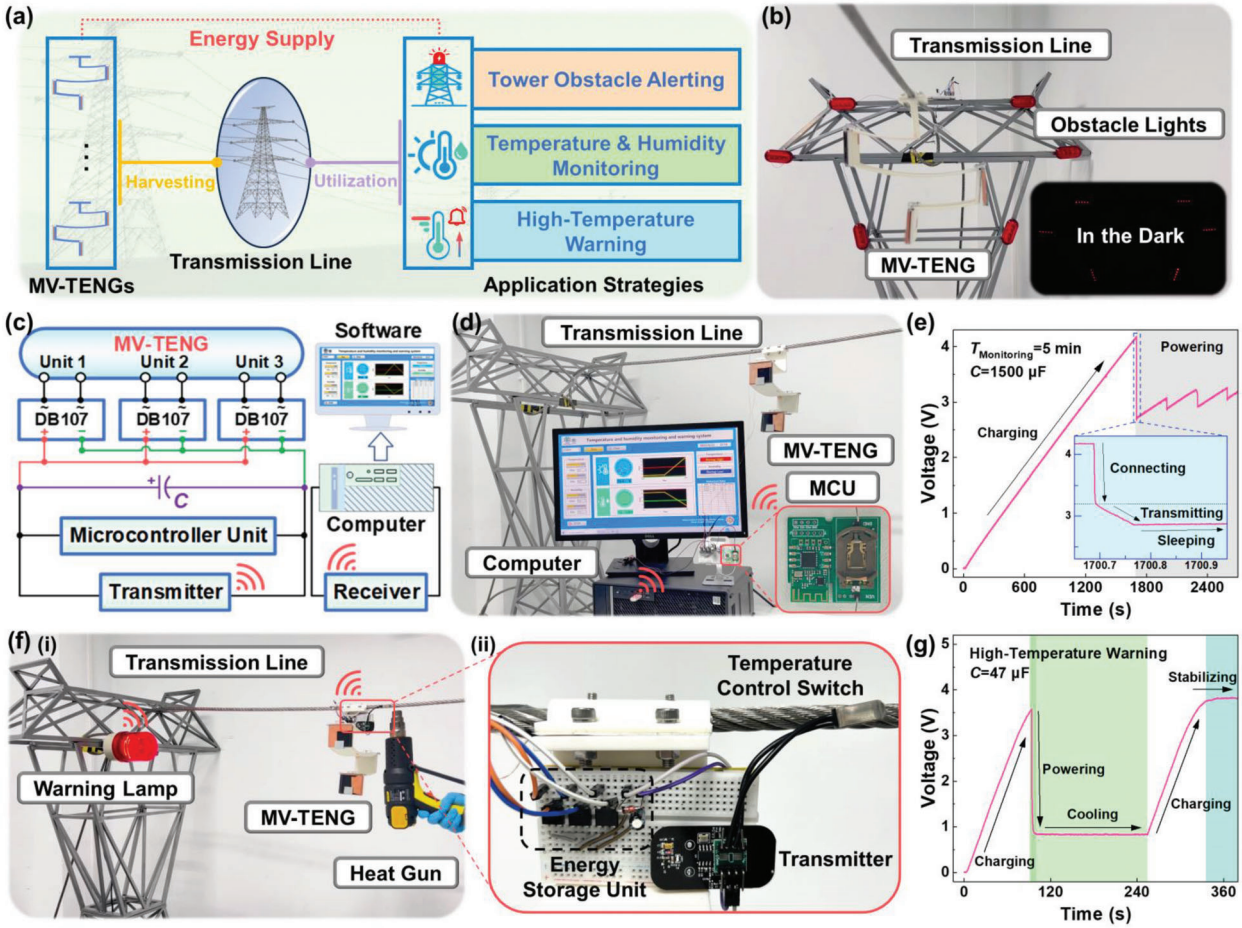

Figure 6. Digital applications of the MV-TENG in the smart transmission lines. a) Block diagram of the MV-TENG for energy harvesting and utilization in transmission lines. b) Application photographs of tower obstacle alerting. c) Circuit diagram, d) application photographs and e) capacitor charging curve of the temperature and humidity monitoring and warning system. f) Application photographs and g) capacitor charging curve of high-temperature warning.

capacitor can be charged to 5 V in 5 s, whereas a 100 μF capacitor needs to take 94 s. It takes 104 s to charge the 100 μF capacitor to 5 V when the vertical vibration frequency is 14 Hz and the amplitude is 3 mm. These results demonstrate the feasibility of the MV-TENG to power various low-power sensing and warning devices in smart transmission lines.

3. Demonstration

Combined with the development trend of digital application of smart transmission lines, three application strategies of self-powered tower obstacle alerting, temperature and humidity online monitoring, and high-temperature wireless warning of transmission line based on the MV-TENG are proposed (**Figure 6**a), and a transmission line simulation system is built according to the actual vibration state of the power transmission system.

First of all, according to the "Convention on International Civil Aviation" and relevant national regulations, aviation obstruction lights need to be installed on transmission lines of 500 kV and above, cross-river transmission lines, and overhead transmission towers near airports and desert areas. The MV-TENG is first installed in the transmission line simulation system, which extracts energy from the vibration of transmission lines and lights up 130 LEDs (diameter of 10 mm), the MV-TENG photographs and application are shown in Figure S12 and Video S3 (Supporting Information). Subsequently, six obstruction lights with LEDs are installed around the contour of the transmission tower model and lit up by the MV-TENG. The shape and height of the tower are marked by obstruction lights so that the aircraft operator can judge the position, height, and contour of the tower to avoid flight accidents. The application system and demonstration process are shown in Figure 6b and Video S4 (Supporting Information). This application proves the feasibility of using TENG to realize self-powered tower obstacle alerting.

In addition, according to the development needs of smart grids, it is necessary to monitor digital information online such as temperature and humidity, wind speed, wind direction, and ice cover conditions of transmission lines to ensure the operation status of transmission lines and the safety of power grid operation. This work builds a wireless monitoring system for online temperature and humidity monitoring and warning in

transmission lines, which combines a low-power wireless temperature and humidity sensor and a software design by LabVIEW. The circuit diagram and software flow of the system are shown in Figure 6c and Figure S13a (Supporting Information). The output energy of the MV-TENG is stored in an electrolytic capacitor via rectifier bridges and powers a wireless microcontroller unit (MCU) equipped with a temperature and humidity sensor. The MCU controls the wireless transmitter to transmit temperature and humidity data to the wireless receiver. The wireless receiver is connected to the computer and provides the data to the temperature and humidity monitoring and warning software designed by LabVIEW through the serial interface. The temperature and humidity are displayed through the software and the alarm is issued when the temperature and humidity exceed the set threshold (Figure S13b, Supporting Information). And all historical monitoring data are also stored in the software. The photographs of the temperature and humidity monitoring and warning system and the voltage of the electrolytic capacitor in operation are shown in Figures 6d,e. Within 30 min, the voltage of the electrolytic capacitor can reach >3.3 V. After the power supply starts, the first connection between the wireless transmitter of the MCU and the wireless receiver on the computer consumes a large amount of energy. Subsequently, after the first data transfer is completed, the MCU goes to sleep. At this time, the sleep current of the MCU is as low as 2 μA, and the energy of the electrolytic capacitor is continuously replenished to meet the subsequent normal operation. The system monitoring period is set to 5 min. The application demonstration process is shown in Video S5 (Supporting Information), which proves the feasibility of adopting TENG to realize all-weather self-powered temperature and humidity online monitoring of transmission lines.

Finally, the excessive wire temperature is a particularly prominent problem affecting the normal operation of transmission lines, which will lead to reduced transmission efficiency and loose joints. To monitor the maximum temperature of transmission line wires and reduce the power consumption and device cost of sensors, this work designs a high-temperature wireless warning system for transmission lines. The circuit principle of the high-temperature wireless warning system is shown in Figure S14 (Supporting Information). Most wires of the overhead network are made of aluminum conductor steel reinforced (ACSR). The operating temperature of ACSR is generally 40–50 °C, and the maximum allowable temperature is ≈70 °C. Therefore, the system is equipped with a 60 °C normally open temperature control switch, and the warning lamp is controlled by a wireless sensing device. The warning lamp can be installed around transmission line towers or in offices on duty. In a laboratory environment, a heat gun is used to heat the wire and then a system warning is triggered. The photographs of the high-temperature wireless warning system of the transmission line and the voltage of the energy storage unit in operation are shown in Figures 6f,g. The MV-TENG charges the voltage of the energy storage unit to >3.3 V within 90 s. The temperature control switch is turned on, and then the wireless warning system is triggered. Subsequently, the voltage of the energy storage unit drops to ≈0.9 V. Since the temperature control switch remains on state until the temperature recovers to 60 °C, the voltage of the energy storage unit remains constant during this period. When the wire temperature drops below 60 °C, the temperature control switch returns to the open state. The voltage of the energy storage unit is replenished, and remains unchanged after reaching the stabilizing value of the zener diode, waiting for the next operation. The application demonstration process is shown in Video S6 (Supporting Information). This application proves the feasibility of using TENG to realize all-weather self-powered wireless high-temperature warning of wires in smart transmission lines.

The successful applications of the above three application strategies meet the actual work requirements of the transmission lines. Considering the scalability of the above application strategies, they can be applied to most TENGs for harvesting wind or vibration energy and other sensing and warning devices with different functions in transmission lines.

4. Conclusion

In summary, combined with the motion characteristics of the cantilever beam and allegro electrodes, an innovative MV-TENG that can realize broadband vibration energy harvesting in two orthogonal directions was proposed. The broadband vibration characteristics of the MV-TENG were verified by modal simulation analysis and experiments. The experimental results show that both arc TENG and MV-TENG could realize large-scale energy harvesting in horizontal and vertical vibration directions. Specifically, the MV-TENG could realize horizontal vibration energy harvesting in the range of 1–3.5 Hz and vertical vibration energy harvesting in the range of 4 Hz and 9–60 Hz, which could meet the frequency range of breeze vibrations and sub-span oscillations. In addition, the coupling output performance of the three units of the MV-TENG was measured. The results indicate that the maximum mean power of the MV-TENG in the horizontal and vertical directions could reach 435.093 and 459.734 μW, respectively. Finally, three application strategies of the MV-TENG in the smart transmission lines are developed. The self-powered tower obstacle alerting, temperature and humidity online monitoring, and high-temperature wireless warning of transmission line based on the MV-TENG were demonstrated separately. The technical feasibility of TENG in the digital application of smart transmission lines was verified. The above work will help to build a clean and low-carbon self-powered intelligent power transmission system to jointly promote the engineering application of the TENG and the digital transformation of the power system.

5. Experimental Section

Fabrication of the MV-TENG: The MV-TENG was mainly composed of S-beam and allegro electrodes. The dimensions of the MV-TENG are 210 mm × 210 mm × 60 mm. The S-beam was made using 3D printing (3DP) technology and was made of PLA. The upper plate electrode was connected to the bottom plate electrode hinge by a steel shaft (diameter of 2 mm). The allegro electrodes used a 0.3 mm thick sponge and 80 μm thick copper foil. The FEP thickness in the bottom plate electrode was 30 mm and the Nylon thickness in the upper plate electrode was 25 mm. The electrodes were connected and output by copper wires (diameter of 0.14 mm). Each PLA plate of the upper plate electrode had a 10 g mass block mounted on the back to increase the movement inertia of the upper plate electrode.

Experimental Measurement: The vibration excitation system was divided into a horizontal vibration excitation system and a vertical vibration excitation system. Among them, the linear motor (Lin Mot, HF01-23) of the horizontal vibration excitation system was installed on

a vibration isolation platform, and the prototype was installed at the front end of the linear motor. The electrodynamic shaker (Labworks Inc., LW139.138-40) of the vertical vibration excitation system was mounted on the vibration isolation platform with the prototype mounted on top. In addition, the output signal generated by the prototype was then acquired by a data acquisition (DAQ) card (NI, USB-6218) and an electrometer (6514, Keithley), and then transferred to a computer where the output signal of the prototype was analyzed and processed by LabVIEW software. It is noteworthy that the coupling voltages output by MV-TENG were measured by an oscilloscope (Tektronix, MDO34).

Application Demonstration: The transmission line simulation system consisted of two 1.5 m high tower models and an aluminum stranded wire (ASW) of 10 mm diameter. The electrodynamic shaker was connected with the ASW to simulate the vibration of the transmission line by controlling the electrodynamic shaker output. Each obstruction light of tower obstacle alerting was equipped with five LEDs with a diameter of 5 mm. The MCU for temperature and humidity online monitoring with a humidity and temperature sensor (SHT35). The transmitter and receiver used ZigBee wireless communication (LRF215). The transmitter and receiver for high-temperature wireless warning of the transmission line were provided by LINPTECH (G6L-TW).

Supporting Information

Supporting Information is available from the Wiley Online Library or from the author.

Acknowledgements

X.Z., Y.Y., and X.X. contributed equally to this work. This research was supported by the Beijing Natural Science Foundation (No. 3222023) and the National Key R&D Project from Minister of Science and Technology (Nos. 2021YFA1201604 and 2021YFA1201601).

Conflict of Interest

The authors declare no conflict of interest.

Data Availability Statement

The data that support the findings of this study are available from the corresponding author upon reasonable request.

Keywords

breeze vibration, multi-mode vibration, smart transmission lines, subspan oscillation, triboelectric nanogenerators

Received: July 21, 2023
Revised: September 6, 2023
Published online:

[1] C. Wietfeld, A. A. Cardenas, H.-H. Chen, P. Popovski, V. W. S. Wong, *IEEE Wirel Commun* **2017**, *24*, 8.
[2] R. Bayindir, I. Colak, G. Fulli, K. Demirtas, *Renew. Sust. Energ. Rev.* **2016**, *66*, 499.
[3] Y. Luo, X. Yu, D. Yang, B. Zhou, *Artif Intell Rev* **2022**, *56*, 173.
[4] J. Lin, B. Zhu, P. Zeng, W. Liang, H. Yu, Y. Xiao, *Wirel. Commun. Mob. Com.* **2015**, *15*, 1799.
[5] H. He, Z. Zhang, Q. Jia, L. Huang, Y. Cheng, B. Chen, *Energy Rep.* **2023**, *9*, 512.
[6] A. B. Alhassan, X. Zhang, H. Shen, H. Xu, *Int. J. Elec. Power* **2020**, *118*, 105862.
[7] Z. L. Wang, *Nano Energy* **2019**, *58*, 669.
[8] X. Zeng, Z. Yang, P. Wu, L. Cao, Y. Luo, *ISIE '95, Proc. IEEE Int. Symp. Ind. Electron.* **2021**, *68*, 7083.
[9] M. M. Werneck, D. M. dos Santos, C. C. de Carvalho, F. V. B. de Nazare, R. C. da, *IEEE Sens. J.* **2015**, *15*, 1338.
[10] L. Zhao, X. Huang, Y. Zhang, Y. Zhu, J. Jia, C. Zhu, *Struct. Control Hlth.* **2020**, *27*, e2538.
[11] L. Zhao, X. Huang, Y. Zhang, Y. Tian, Y. Zhao, *Electronics-Switz* **2019**, *8*, 515.
[12] F.-R. Fan, Z.-Q. Tian, Z. Lin Wang, *Nano Energy* **2012**, *1*, 328.
[13] Z. L. Wang, *Rep Prog Phys* **2021**, *84*, 096502.
[14] M. Yin, X. Lu, G. Qiao, Y. Xu, Y. Wang, T. Cheng, Z. L. Wang, *Adv. Energy Mater.* **2020**, *10*, 2000627.
[15] C. Wang, H. Guo, P. Wang, J. Li, Y. Sun, D. Zhang, *Adv. Mater.* **2023**, *35*, 2209895.
[16] Z. L. Wang, *Faraday Discuss.* **2014**, *176*, 447.
[17] H. Wen, X. Yang, R. Huang, D. Zheng, J. Yuan, H. Hong, J. Duan, Y. Zi, Q. Tang, *Adv. Sci.* **2023**, *10*, 2302009.
[18] X. Zhang, H. Li, Q. Gao, Z. Yuan, S. He, X. Yu, Z. L. Wang, T. Cheng, *Nano Energy* **2023**, *108*, 108239.
[19] B. Chen, Y. Yang, Z. L. Wang, *Adv. Energy Mater.* **2018**, *8*, 1702649.
[20] L. He, C. Zhang, B. Zhang, O. Yang, W. Yuan, L. Zhou, Z. Zhao, Z. Wu, J. Wang, Z. L. Wang, *ACS Nano* **2022**, *16*, 6244.
[21] J.-H. Son, S.-H. Chung, K. Cha, S. Kim, Z.-H. Lin, J. Hong, J. Chung, S. Lee, *Adv. Mater.* **2023**, *35*, 2300283.
[22] B. D. Chen, W. Tang, C. He, C. R. Deng, L. J. Yang, L. P. Zhu, J. Chen, J. J. Shao, L. Liu, Z. L. Wang, *Mater. Today* **2018**, *21*, 88.
[23] Z. Qu, M. Huang, C. Chen, Y. An, H. Liu, Q. Zhang, X. Wang, Y. Liu, W. Yin, X. Li, *Adv. Funct. Mater.* **2022**, *32*, 2202048.
[24] X. Xiao, X. Zhang, S. Wang, H. Ouyang, P. Chen, L. Song, H. Yuan, Y. Ji, P. Wang, Z. Li, M. Xu, Z. L. Wang, *Adv. Energy Mater.* **2019**, *9*, 1902460.
[25] W. Guo, Y. Long, Z. Bai, X. Wang, H. Liu, Z. Guo, S. Tan, H. Guo, Y. Wang, Y. Miao, *Energ. Convers. Manage.* **2022**, *268*, 115969.
[26] T. Du, F. Dong, Z. Xi, M. Zhu, Y. Zou, P. Sun, M. Xu, *Small* **2023**, *19*, e2300401.
[27] Y. Yu, H. Li, D. Zhao, Q. Gao, X. Li, J. Wang, Z. L. Wang, T. Cheng, *Mater. Today* **2023**, *64*, 61.
[28] J. Han, Y. Liu, Y. Feng, T. Jiang, Z. L. Wang, *Adv. Energy Mater.* **2022**, *13*, 2203219.
[29] S. Zhang, Z. Jing, X. Wang, K. Fan, H. Zhao, Z. L. Wang, T. Cheng, *ACS Energy Lett.* **2022**, *7*, 4282.
[30] B. Godard, S. Guerard, J.-L. Lilien, *IEEE T. Power Deliver* **2011**, *26*, 2111.
[31] L. Zhao, X. Huang, Y. Zhao, W. Si, *Struct. Control Hlth.* **2018**, *25*, e2143.
[32] H. Wu, J. Wang, Z. Wu, S. Kang, X. Wei, H. Wang, H. Luo, L. Yang, R. Liao, Z. L. Wang, *Adv. Energy Mater.* **2022**, *12*, 2103654.
[33] X. Tong, Y. Tan, P. Zhang, Y. Cao, Y. Wang, X. Li, L. Ren, T. Cheng, *Sustain. Energ. Fuels* **2022**, *6*, 4197.
[34] C. He, T. Yang, J. Fang, X. Pu, K. Shang, G. Tian, X. Lu, J. Wu, W. Yang, L. Qian, *Nano Energy* **2023**, *109*, 108279.
[35] S. Hu, Z. Yuan, R. Li, Z. Cao, H. Zhou, Z. Wu, Z. L. Wang, *Nano Lett.* **2022**, *22*, 5584.
[36] S. Gao, X. Zeng, G. Zhang, J. Zhang, Y. Chen, S. Feng, W. Lan, J. Zhou, Z. L. Wang, *Nano Energy* **2022**, *101*, 107530.
[37] W. Xie, T. Peng, K. Xiao, J. Zhang, *Int. J. Eng. Technol. In.* **2017**, *9*, 437.
[38] G. Diana, M. Belloli, S. Giappino, A. Manenti, L. Mazzola, S. Muggiasca, A. Zuin, *IEEE T. Power Deliver* **2014**, *29*, 1311.